Effect of time-varying flow-shear on the nonlinear stability of the boundary of magnetized toroidal plasmas

Youngmin Oh, Hyung Ju Hwang, Michael Leconte, Minwoo Kim, and Gunsu S. Yun

Citation: AIP Advances **8**, 025224 (2018); doi: 10.1063/1.5006554
View online: https://doi.org/10.1063/1.5006554
View Table of Contents: http://aip.scitation.org/toc/adv/8/2
Published by the American Institute of Physics

Effect of time-varying flow-shear on the nonlinear stability of the boundary of magnetized toroidal plasmas

Youngmin Oh,[1,a] Hyung Ju Hwang,[2,b] Michael Leconte,[3,c] Minwoo Kim,[4,d] and Gunsu S. Yun[5,e]

[1]*Beijing Computational Science Research Center, Beijing 100193, China*
[2]*Department of Mathematics, Pohang University of Science and Technology, Pohang, Gyeongbuk 37673, Republic of Korea*
[3]*National Fusion Research Institute, Daejeon 34133, Republic of Korea*
[4]*School of Natural Science, Ulsan National Institute of Science and Technology, Ulsan 44919, Republic of Korea*
[5]*Department of Physics, Pohang University of Science and Technology, Pohang, Gyeongbuk 37673, Republic of Korea*

(Received 26 September 2017; accepted 19 February 2018; published online 28 February 2018; corrected 6 March 2018)

We propose a phenomenological yet general model in a form of extended complex Ginzburg-Landau equation to understand edge-localized modes (ELMs), a class of quasi-periodic fluid instabilities in the boundary of toroidal magnetized high-temperature plasmas. The model reproduces key dynamical features of the ELMs (except the final explosive relaxation stage) observed in the high-confinement state plasmas on the Korea Superconducting Tokamak Advanced Research: quasi-steady states characterized by field-aligned filamentary eigenmodes, transitions between different quasi-steady eigenmodes, and rapid transition to non-modal filamentary structure prior to the relaxation. It is found that the inclusion of time-varying perpendicular sheared flow is crucial for reproducing all of the observed dynamical features. https://doi.org/10.1063/1.5006554

I. INTRODUCTION

Relaxation phenomena in magnetized plasmas are widespread in nature.[1,2] A notable example is the explosive flares on the surface of the Sun. Another example is the semi-periodic explosive bursts appearing at the boundary of toroidally-confined high-temperature plasmas (e.g., tokamak). In toroidal magnetic confinement devices, sufficient heating of the plasma can lead to a transition from low-confinement state (L-mode) to high-confinement state (H-mode) if the heating power exceeds a threshold. During the transition, a transport barrier (called pedestal) spontaneously appears at the edge of plasma via strong $E \times B$ flow shear which reduces heat and particle transports. However, this barrier is quite unstable and prone to a class of fluid instabilities called edge-localized modes (ELMs) driven by the large gradient of density, temperature, current density, and flow.[3–8] It is believed that these instabilities are responsible for the relaxation (or crash) of the transport barrier, i.e., rapid expulsion of heat and particles. The expulsion events are commonly called ELM crash. The H-mode plasmas are characterized by semi-periodic cycles between slow transport barrier buildup and its fast relaxation.

The ELM crash must be controlled because the natural or uncontrolled crashes induce significant heat and particle fluxes which can damage the plasma-facing walls of the confinement device.

[a]Electronic mail: youngminoh19850329@csrc.ac.cn
[b]Electronic mail: hjhwang@postech.ac.kr
[c]Electronic mail: mleconte@nfri.re.kr
[d]Electronic mail: minwookim@unist.ac.kr
[e]Electronic mail: (corresponding) gunsu@postech.ac.kr

Magnetic perturbations have been used successfully to mitigate or suppress the crash[9–11] but the underlying mechanisms of mitigation and suppression are still unclear. Accordingly, it is crucial to understand the dynamics of ELM for more reliable and robust methods to avoid the crash. For this reason, a nonlinear mathematical analysis is required beyond linear stability analyses.[12]

For the purpose of studying the nonlinear behavior, a nonlinear model for the perturbed pressure was derived in a form of complex Ginzburg-Landau equation based on a 1D reduced MHD model.[13] The numerical solutions to the model equation showed nonlinear relaxation oscillations with the characteristics of type-III ELM. Inspired by Ref. 13, we mathematically studied the model equation to understand the effect of perpendicular flow shear on the nonlinear behavior of the perturbed pressure during the ELM cycle.[14] More precisely, it was shown that there exists a linearly stable symmetric steady state for small shear and the first eigenvalues of unstable states for the case of zero shear are bounded below by a positive constant. In the case of large shear, a theoretical clue was found for the long-time behavior of the solutions: 1) nonlinear oscillation; 2) convergence to 0. The theoretical results were supported by numerical verifications.

However, in Ref. 14, the shear strength was set constant in time, which was insufficient to explore clues for the various phenomena observed in experiments on the Korea Superconducting Tokamak Advanced Research (KSTAR) device such as quasi-steady state with a single eigenmode-like structure[15] and fast transitions between the quasi-steady states.[16] In this paper, the effect of time-varying flow shear is analyzed as the key for accessing different dynamical states. The remaining of the article is organized as follows. In section II, we present the analysis of the model for the case of a single-mode. In section III, we extend the model to treat the case of two coupled modes. In section IV, we discuss the results and give a conclusion with a prospect for comparison with future numerical simulation including the effect of time-varying flow shear.

II. ANALYSIS OF SINGLE-MODE

We consider the following single-mode equation for the perturbed pressure $P(t, x, y)$ in cylindrical magnetized plasma assuming local slab geometry with the magnetic field direction z, the local radial direction x, and the perpendicular direction y:

$$\partial_t P + \gamma_N |P|^2 P = iAW_K(x) P + \gamma_L P + \eta \partial_x^2 P, \tag{1}$$

where $W_K(x) = \tanh(Kx)$ is the prescribed shear flow with $x \in [-1, 1]$, $K > 0$ is the inverse of the shear layer width, and $A \geq 0$ is the shear flow strength. Eq. (1) may be considered an extension of Ginzburg-Landau equation (GLE) with constant complex coefficients. Note that P represents the complex-valued amplitude of a Fourier mode, i.e. $\delta P(x, y, t) = P(x, t)e^{iky} + c.c.$ Here, γ_N, γ_L and η are constant coefficients for the nonlinear, the linear growth and the dissipative terms respectively. It was observed that the behavior of a solution to Eq. (1) is completely different with the presence of the flow-shear for both the Dirichlet and Neumann boundary conditions.[13,14] Since it is unclear which boundary condition is reasonable in real experiments, both types of boundary conditions are considered here to understand the long-time behavior of a solution $P(t, x)$ to Eq. (1):

$$P(t, \pm 1) = 0 \text{ (Dirichlet)},$$
$$\frac{\partial P}{\partial x}(t, \pm 1) = 0 \text{ (Neumann)}.$$

Inspired by Ref. 14, we will consider two subjects for the model Eq. (1). The first subject is to characterize the long-time behavior of a solution $P(t, x)$ for the fixed large shear strength A so that we can distinguish the regions of either convergence to 0 or nonlinear oscillations in the γ_L–η parameter space. The second subject is to characterize the long-time behavior of a solution $P(t, x)$ between nonlinear oscillations and convergence to nontrivial steady states in the A–K parameter space under suitable fixed parameters γ_L and η such that non-trivial solutions are guaranteed. We find a threshold $A_K > 0$ for each K such that solutions converge to a nonzero steady state of Eq. (1) for $A < A_K$ and nonlinearly oscillate for $A > A_K$. Combining these results, we propose that the salient features of the ELM dynamics observed in the KSTAR H-mode plasmas can be explained based on time-varying perpendicular shear flow.

A. Long-time behavior of $P(t, x)$ on γ_L and η

Notice that the Dirichlet boundary condition does not allow nonzero uniform steady states of Eq. (1) even without the shear in contrast with the Neumann boundary condition. Nevertheless, we obtained similar results for both boundary conditions. Fig. 1 represents the long-time behaviors of a solution $P(t, x)$ on γ_L and η for a fixed large $A = 50$ in both boundary conditions. The blue regions in Fig. 1(a)–(b) display that $P(t, x)$ converges to 0 as $t \to \infty$. Conversely, red regions in Fig. 1(*a*)–(*b*) display that $P(t, x)$ oscillates nonlinearly in time. These results show a certain relation between η and γ_L which determines the long-time behavior of $P(t, x)$. Inspecting Fig. 1, it is clear that nonlinear oscillations are guaranteed only if the ratio γ_L/η is sufficiently large. Otherwise, $P(t, x)$ converges to 0. Note that the parameters in Eq. (1) are related to heat flux Q as (see Ref. 13),

$$\gamma_L = \gamma_{L0}\frac{Q - Q_c}{\eta} a p_0^{-1}, \ \gamma_N = a^2\gamma_{L0}^2/\eta, \ \text{ and } \frac{\gamma_L}{\eta} \propto \gamma_{L0}\frac{Q - Q_c}{\eta^2}.$$

where Q_c is the threshold heat flux related to the critical pressure gradient for linear instability, p_0 is the reference pressure, and a denotes the radius of the cylinder (see Ref. 13 for detail). Therefore, even if the heat flux Q exceeds the linear threshold Q_c, nonlinear oscillations may not occur if $0 < Q - Q_c \ll 1$ such that $\gamma_L \ll 1$ and $(\gamma_L/\eta) \ll 1$. This is consistent with experiment observations since it is known that ELM crash does not immediately occur after Q exceeds Q_c (see Fig. 1 in Ref. 17). It is also possible to interpret the case of $Q - Q_c < 0$ ($\gamma_L < 0$) as L-mode. $\gamma_L < 0$ guarantees the long time behavior of $P(t, x)$ such that $\lim_{t\to\infty} |P(t, x)| \to 0$. Therefore, Eq. (1) provides a reasonable explanation of the overall ELM dynamics.

We need to discuss the effect of γ_N. Our expectation is that the stability of the zero solution is crucial to determine the long-time dynamics of $P(t, x)$ for a fixed $A \gg 1$. In consideration of the analysis result in Ref. 14, it is natural to think that $P(t, x)$ will oscillate nonlinearly if the zero solution is unstable, but converge to 0 if the zero solution is stable. For this prediction, we linearized Eq. (1) around the zero solution $P = 0$ and proved that the stability of the zero solution is independent of γ_N, as expected:

$$\partial_t P_L = iAW_K(x) P_L + \gamma_L P_L + \eta\partial_x^2 P_L. \tag{2}$$

Accordingly, it is reasonable to expect that γ_N cannot affect the long-time behavior of the zero solution for large $A > 0$. Conversely, γ_N is expected to affect the long-time behavior of the non-zero solution for large $A > 0$. Under this prediction, we confirmed numerically that γ_N does not affect the qualitative long-time behavior of the solutions illustrated in Fig. 1(*a*)–(*b*). Instead, γ_N can affect the amplitude of nonlinear oscillations. The change of the amplitude $|P(t, 0)|$ in our model is strongly associated with $(\gamma_L/\gamma_N)^{1/2} = \frac{1}{a}\left(\frac{p_{\text{ref}}}{\gamma_{L0}}(Q - Q_c)\right)^{1/2}$.

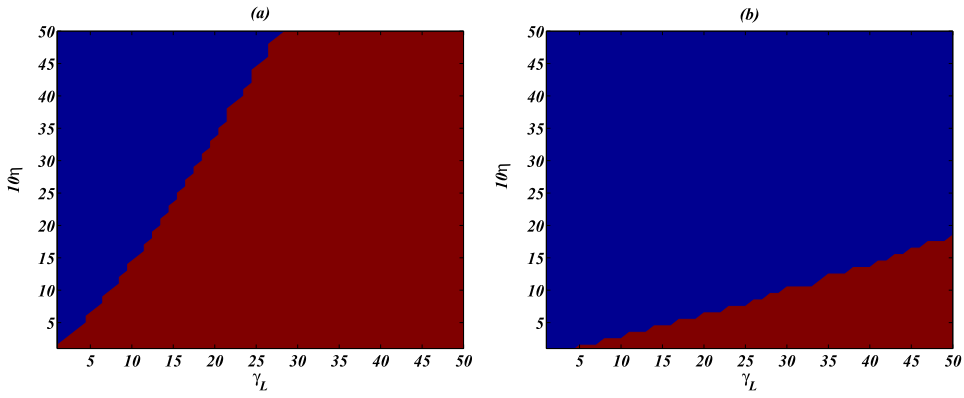

FIG. 1. The qualitative long-time behavior of a solution $P(t, x)$ to Eq. (1): nonlinear oscillation (red regions) or convergence to 0 (blue regions) on the Neumann and the Dirichlet boundary conditions in (*a*) and (*b*) respectively. Here, we set $\gamma_N = 1$, $A = 50$, and $W_K(x) = \tanh(25x)$. In each case, there exists a clear boundary separating the two regions.

B. Long-time behavior of $P(t, x)$ on A and K

Fig. 2 suggests that there exists a threshold flow shear amplitude A_K for given K for both boundary conditions. If $0 < A < A_K$ (blue regions), the solution $P(t, x)$ converges to a nonconstant steady state $P_s(x)$ for any given initial condition. On the other hand, the qualitative long-time behavior of $P(t, x)$ abruptly changes if $A > A_K$ (red regions). $P(t, x)$ oscillates nonlinearly and never converges to any steady state in the red regions. These numerical results show that there is a certain stability/instability criterion A_K of A for each $K > 0$ for both boundary conditions. According to Fig. 2, we can also predict that ELM crash only occurs under sufficiently strong flow shear. We can also observe that as approaching the threshold line in Fig. 2, the amplitude of nonlinear oscillations (in the red regions) increases and the central value $|P(0)|$ for a nonzero steady state $P(x)$ (in the blue regions) decreases but remain finite (i.e. nonzero). Besides, it is also observed that A_K and K are inversely correlated for small K for both boundary conditions, but A_K barely changes for large K.

Mathematical clues for the two different dynamic behaviors illustrated in Figs. 1 and 2 can be explained in the case of the Neumann boundary condition. Let $P(t, x) = R(t, x) \exp(i\theta(t, x))$ to rewrite Eq. (1) as:

$$\partial_t R = \gamma_L R + \eta \partial_x^2 R - \eta R \theta'^2 - \gamma_N R^3, \tag{3}$$

$$\partial_t \theta = \eta \partial_x \theta' + 2\eta(\partial_x \ln R)\theta' - AW_K(x), \tag{4}$$

where $\theta' = \partial_x \theta$. In Eq. (3), the shear term $AW_K(x)$ affects the amplitude R only indirectly via the phase-gradient θ'. Without flow-shear ($A = 0$), the steady-state $P = (\gamma_L/\gamma_N)^{1/2}$ is the only stable equilibrium.[18] Hence, without flow-shear, the phase-gradient θ' converges to 0. However, for finite flow-shear, the term $\eta R\theta'^2$ in Eq. (3) is nonzero and causes R to decay in time. If the shear is large, the term $\eta R\theta'^2$ dominates the linear growth term $\gamma_L R$ in a neighborhood of $x = 0$, so $R(t, 0)$ decays due to the phase-gradient θ' until a critical phase-gradient $\theta' = \theta'_c$ is reached. After decaying, however, the term $\gamma_N R^3$ is weak close to 0 and the term $\eta \partial_x^2 R$ grows so large that $R(t, 0)$ tends to return to its original state with the help of the linear drive $\gamma_L R$. This interaction between decay and growth terms makes the nonlinear oscillation. However, if γ_L is too small, i.e., the mode is linearly stable, the term $\eta \partial_x^2 R$ is insufficient to fully dominate the term $\eta R\theta'^2$. Accordingly, it is impossible to return to the initial state and $R(t, x)$ converges to 0 instead. Similar explanations for the behavior of nonlinear

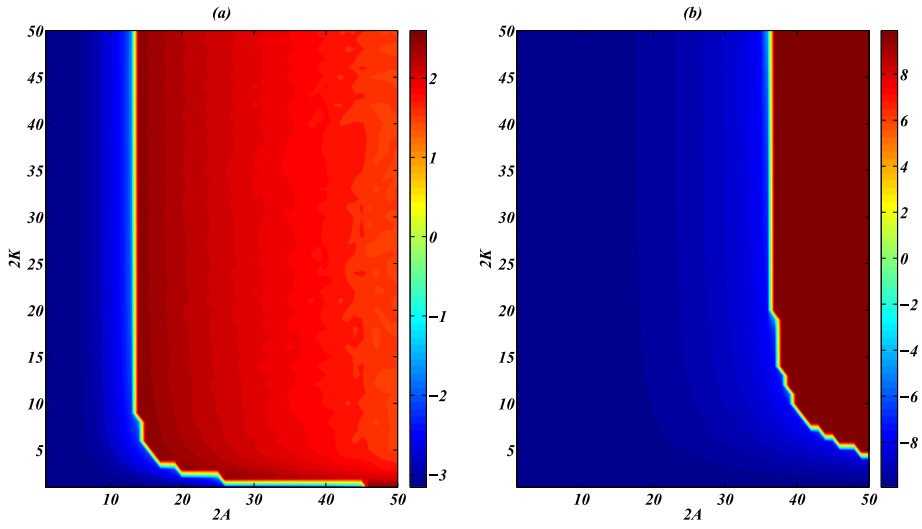

FIG. 2. The qualitative long-time behavior of a solution $P(t, x)$ to (1) with $\eta = 1$, $\gamma_N = 1$, and $\gamma_L = 10$: nonlinear oscillation (red regions) or convergence to a nonzero steady state (blue regions) for the Neumann and the Dirichlet boundary conditions in (a)-(b) respectively: The values in the red regions in (a)-(b) denote $\lim_{t\to\infty} \max |P(t, 0)|$. The values in the blue regions (a)-(b) denote $-|P(0)|$ for a nonzero steady state $P(t, x) = P(x)$. It is clear that there is A_K for each K which determines the long-time behavior of the solution. Note that, as approaching the interfaces, the values in the red and blue regions increase, so the amplitude of nonlinear oscillations increases and $|P(0)|$ for a nonzero steady state $P(x)$ decreases, but not to 0.

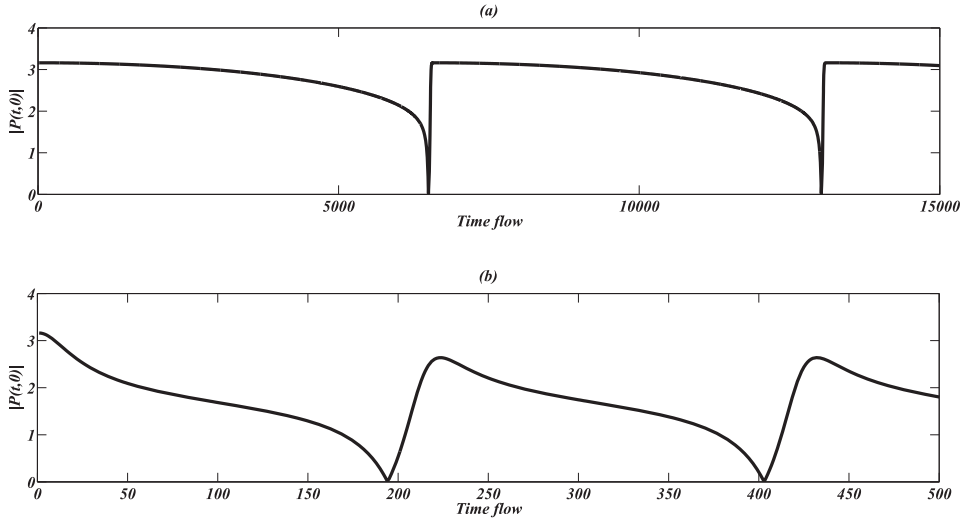

FIG. 3. The time behaviors of the amplitude $|P(t,0)|$ of the solution $P(t, x)$ to Eq. (1) with $\gamma_N = 1$, $\gamma_L = 10$, $\eta = 1$, $W(x) = \tanh(25x)$ on the Neumann boundary condition. The initial condition is $P(0,x) = (\gamma_L/\gamma_N)^{1/2} \cos\left(\frac{\pi x}{2}\right)$. (a) $A(t)$ is modeled such that A increases linearly on time from 0 initially but decreases to 0 rapidly after the transition (crash) which occurs at $A \approx 6.5$, and this procedure is repeated. (b) $A = 6.5$ is constant. The quasi-steady state is only observed in (a).

oscillations were introduced in Refs. 13 and 14. In addition, it can be proved that K is not an important parameter in Fig. 2 for $K \gg 1$ [c.f. Appendix].

C. The effect of time-varying *A*

Nevertheless, we could not observe non-oscillating quasi-steady state for the prescribed shear flow $AW_K(x)$ for both boundary conditions when $A > A_K$. The existence of a quasi-steady state is important for the validation of our model because the ELM dynamics observed on the KSTAR consists of distinctive stages including quasi-steady states, transition phase, and crash phase.[15] We believe that it is impossible to obtain a quasi-steady state for time-independent coefficients. Indeed, if $|\partial P_L/\partial t| \ll 1$, then a solution should be close to a steady state. However, there is no reasonable

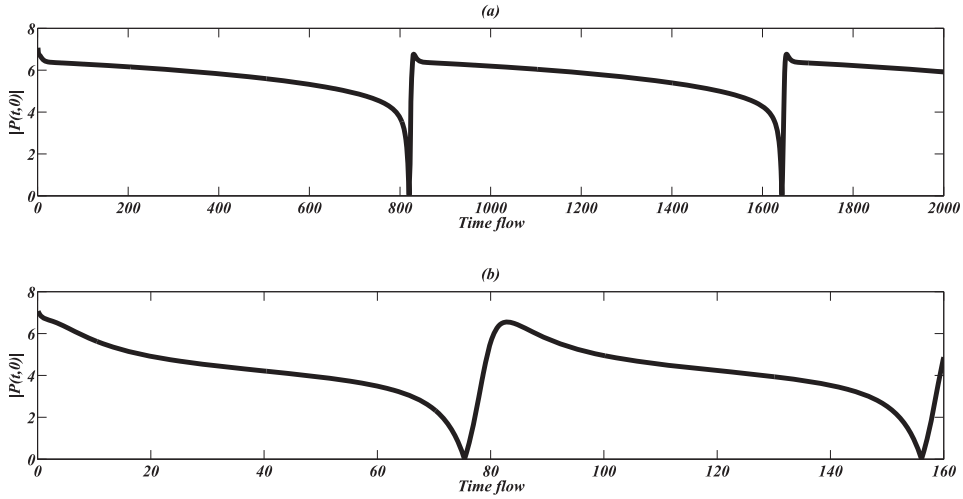

FIG. 4. The time behaviors of the amplitude $|P(t,0)|$ of the solution $P(t,x)$ to (1) with $\gamma_N = 1, \gamma_L = 50, \eta = 1, W(x) = \tanh(25x)$ on the Dirichlet boundary conditions. The initial condition is $P(0,x) = (\gamma_L/\gamma_N)^{1/2} \cos\left(\frac{\pi x}{2}\right)$. (a) $A(t)$ is modeled such that A increases linearly on time from 10 initially but decreases to 10 rapidly after the transition (crash) which occur at $A \approx 18$, and this procedure is repeated. (b) $A = 18$ is constant. The quasi-steady state is only observed in (a).

steady state $P^s_{A,K}$ (such that $\partial_x P^s_{A,K}(x) \le 0$ in $0 \le x \le 1$ and $\partial_x P^s_{A,K}(x) \ge 0$ in $-1 \le x \le 0$) for a sufficiently large fixed shear,[14] so we cannot expect a quasi-steady state. In real experiment, it is natural to think that shear flow evolves, i.e., A and K vary in time. Thus, it makes sense that in the quasi-steady state phase, the parameters A and K are initially located in a region where solutions converge to a steady state (blue regions in Fig. 2), but as time flows, a shear flow gradually increases, and A and K gradually change. As a consequence, as A exceeds the critical point A_K, i.e., A moves from the blue regions to the red regions in Fig. 2, the quasi-steady state can no longer exist, which may amount to the sudden crash observed in each ELM cycle.

The existence of quasi-steady states with time-varying $A(t)$ is numerically illustrated in Figures 3 and 4 for both boundary conditions. These numerical examples suggest that the change of A induces different stages in the ELM dynamics. Based on these results, we expect that magnetic perturbations can reduce the shear flow strength A such that quasi-steady ELMs can persist without crash, which would correspond to the suppression (absence) of ELM crashes.

III. ANALYSIS OF COUPLED MODES

In this section, we consider two coupled modes with the Neumann boundary condition to study the mode transitions during the quasi-steady observed on the KSTAR.[16] Let $W(x)$ be a prescribed shear flow profile and the pressure P be written as

$$P = \overline{P} + \widetilde{P},$$

where $\overline{P} = \overline{P}(t,x)$ is the slowly time-varying equilibrium pressure and $\widetilde{P} = \widetilde{P}(t,x,y)$ is the pressure perturbation:

$$\widetilde{P} = P_1 \exp(ik_1 y) + P_2 \exp(ik_2 y) + c.c., \tag{5}$$

with $|k_1| \neq |k_2|$. Extending the single mode model in Ref. 13, we consider the following model:

$$\frac{\partial P_1}{\partial t} - \eta \frac{\partial^2 P_1}{\partial x^2} + ik_1 A W(x) P_1 = -b\left(\frac{\partial \overline{P}}{\partial x} P_1\right) + C_1 P_1, \tag{6}$$

$$\frac{\partial P_2}{\partial t} - \eta \frac{\partial^2 P_2}{\partial x^2} + ik_2 A W(x) P_2 = -b\left(\frac{\partial \overline{P}}{\partial x} P_2\right) + C_2 P_2, \tag{7}$$

$$\frac{\partial \overline{P}}{\partial t} + c\frac{\partial}{\partial x}\left(\int_0^1 |\widetilde{P}|^2 dy\right) = d\frac{\partial^2 \overline{P}}{\partial x^2}, \tag{8}$$

where $\eta > 0$, $A > 0$, $b > 0$, $c > 0$, $d > 0$, $C_1 \ge 0$, and $C_2 \ge 0$ are constants. With the help of the slaving approximation $\left(\frac{\partial \overline{P}}{\partial t} \approx 0\right)$,[13] we can obtain

$$\frac{c\left(|P_1|^2 + |P_2|^2\right) - e}{d} = \frac{\partial \overline{P}}{\partial x} \tag{9}$$

from Eq. (8) for a constant $e \in \mathbb{R}$ using $\int_0^1 |\widetilde{P}|^2 dy = |P_1|^2 + |P_2|^2$. Therefore, substituting Eq. (9) into Eqs. (6)–(7) yields

$$\frac{\partial P_1}{\partial t} - \eta \frac{\partial^2 P_1}{\partial x^2} + iAk_1 W(x) P_1 = -b\left(\frac{c\left(|P_1|^2 + |P_2|^2\right) - e}{d}\right) P_1 + C_1 P_1, \tag{10}$$

$$\frac{\partial P_2}{\partial t} - \eta \frac{\partial^2 P_2}{\partial x^2} + iAk_2 W(x) P_2 = -b\left(\frac{c\left(|P_1|^2 + |P_2|^2\right) - e}{d}\right) P_2 + C_2 P_2, \tag{11}$$

Denoting

$$\gamma_N := \frac{bc}{d},$$

$$\gamma_{L_1} := \left(\frac{be}{d} + C_1\right),$$

$$\gamma_{L_2} \coloneqq \left(\frac{be}{d} + C_2\right),$$

we can rewrite Eqs. (10)–(11) as

$$\frac{\partial P_1}{\partial t} - \eta \frac{\partial^2 P_1}{\partial x^2} + iAk_1 W(x) P_1 = -\gamma_N P_1 \left(|P_1|^2 + |P_2|^2\right) + \gamma_{L_1} P_1, \tag{12}$$

$$\frac{\partial P_2}{\partial t} - \eta \frac{\partial^2 P_2}{\partial x^2} + iAk_2 W(x) P_2 = -\gamma_N P_2 \left(|P_1|^2 + |P_2|^2\right) + \gamma_{L_2} P_2. \tag{13}$$

Let $P_1 = R_1 \exp(i\theta_1)$ and $P_1 = R_2 \exp(i\theta_2)$. Then Eqs. (12)–(13) can be written as

$$\dot{R}_1 - \eta R_1'' + \eta R_1 \theta_1'^2 = -\gamma_N \left(R_1^3 + R_1 R_2^2\right) + \gamma_{L_1} R_1,$$

$$\dot{R}_2 - \eta R_2'' + \eta R_2 \theta_2'^2 = -\gamma_N \left(R_2^3 + R_1 R_2^2\right) + \gamma_{L_2} R_2$$

We assume that $\gamma_{L_1} \neq \gamma_{L_2}$. Here, we can interpret γ_N, $\gamma_{L_1}, \gamma_{L_2}$ and η as constant coefficients for the nonlinear term, the linear growth terms for P_1 and P_2, and the dissipative term respectively. In this paper, we only consider positive values of $\gamma_{L_1}, \gamma_{L_2}, \eta$ and γ_N. The only difference from Eq. (1) to Eqs. (12)–(13) is the presence of the coupling terms $\gamma_N P_1 |P_2|^2$ and $\gamma_N P_2 |P_1|^2$ in the equations for P_1 and P_2 respectively, which can account for the mode transition observed in Ref. 16.

A. Long-time behavior on the linear growth terms

To understand the dependence of the time behavior of the couple modes on the linear growth terms, we performed numerical calculations with fixed $\eta = \gamma_N = 1$, $A = 10$, $W(x) = \tanh(25x)$, $k_1 = 5$ and $k_2 = 8$ for different $\gamma_L's$. Fig. 5 shows the time behaviors of $|P_1(t,0)|$ and $|P_2(t,0)|$ for $\gamma_{L_1} = 30$ and $\gamma_{L_2} = 20$ with the initial condition $|P_1(0,x)| \ll |P_2(0,x)|$. $|P_1(t,0)|$ grows and becomes dominant with nonlinear oscillation while $|P_2(t,0)|$ decays. Fig. 6 shows the case for $\gamma_{L_1} = 15$ and $\gamma_{L_2} = 20$ with the opposite initial condition $|P_1(0,x)| \gg |P_2(0,x)|$. $|P_1(t,0)|$ converges to 0 and $|P_2(t,0)|$ becomes dominant as $t \to \infty$.

In both cases, the mode with higher γ_L becomes dominant eventually as expected. However, there is a subtle difference in the time scale between Fig. 5 and Fig. 6. We can explain the difference as follows. For the case of Fig. 5, $\gamma_{L_1} > \gamma_{L_2}$ and $|k_1| < |k_2|$ mean that P_1 has stronger linear growth and, at the same time, less suppression due to the shear compared to P_2 so that P_1 will quickly become dominant. However, in the case of Fig. 6, although $\gamma_{L_1} < \gamma_{L_2}$, it takes longer for P_2 to become dominant because P_1 is less suppressed than P_2 by the shear.

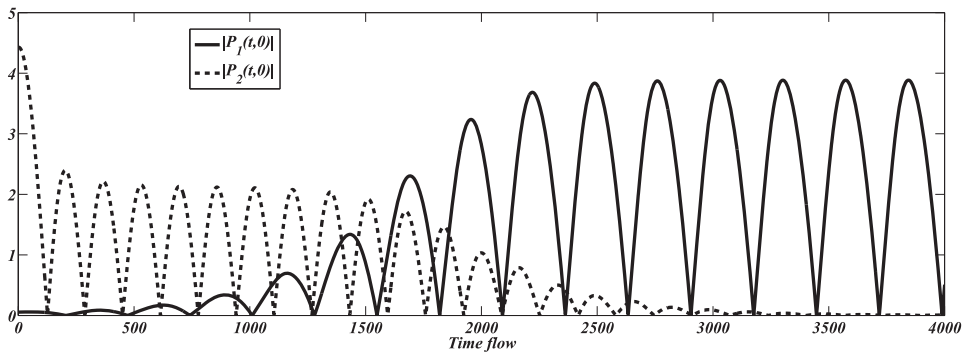

FIG. 5. The time behaviors of $|P_1(t,0)|$ and $|P_2(t,0)|$, where $P_1(t,x)$ and $P_2(t,x)$ are solutions to Eqs. (12), (13) respectively. We set $\eta = 1$, $A = 10$, $k_1 = 5$, $k_2 = 8$, $\gamma_N = 1$ and $W(x) = \tanh(25x)$. Besides, we imposed $\gamma_{L_1} = 30$ and $\gamma_{L_2} = 20$ and initial conditions $P_1(0,x)$ and $P_2(0,x)$ as $\left(\frac{\gamma_{L_1}}{\gamma_N}\right)^{1/2}(0.01)$ and $\left(\frac{\gamma_{L_2}}{\gamma_N}\right)^{1/2}(0.99)$ respectively. $|P_1(t,0)|$ becomes dominant and oscillates nonlinearly although the initial value is small while $|P_2(t,0)|$ converges to 0 although the initial value is large. Hence, the conditions $\gamma_{L_1} > \gamma_{L_2}$ and $k_1 < k_2$ means the dominance of $|P_1(t,0)|$ for sufficiently large shear.

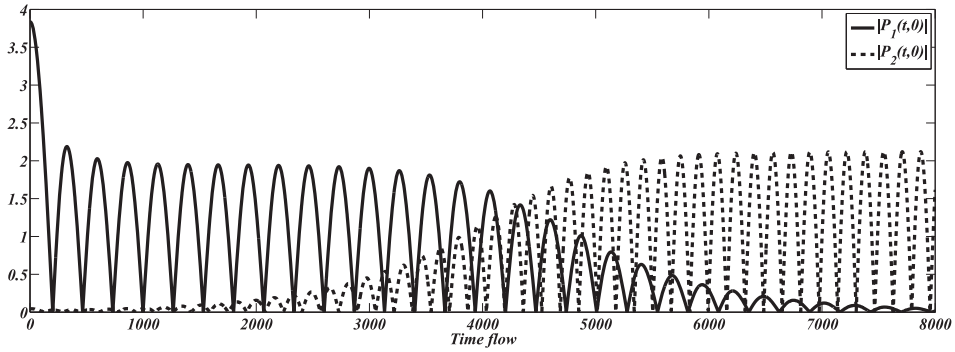

FIG. 6. The time behaviors of $|P_1(t,0)|$ and $|P_2(t,0)|$ where $P_1(t,x)$ and $P_2(t,x)$ are solutions to Eqs. (12), (13) respectively. We set the same values for the parameters $\eta, A, k_1, k_2, \gamma_N$, and $W(x)$ as in Fig. 5. Besides, we imposed $\gamma_{L_1} = 15$ and $\gamma_{L_2} = 20$ and initial conditions $P_1(0, x)$ and $P_2(0, x)$ as $\left(\frac{\gamma_{L_1}}{\gamma_N}\right)^{1/2}(0.99)$ and $\left(\frac{\gamma_{L_2}}{\gamma_N}\right)^{1/2}(0.01)$ respectively. $|P_1(t,0)|$ converges to 0 and $|P_2(t,0)|$ oscillates nonlinearly, showing that the linear growth terms highly affect the long-time behavior of the two modes.

To conclude, the long-time behaviors of $|P_1|$ and $|P_2|$ under 'fixed' parameters with $k_1 < k_2$ are determined by γ_{L_1} and γ_{L_2}.

B. Long-time behavior for time-varying *A*

The analysis shown in Figs. 5–6 still cannot explain the transitions between quasi-stable modes observed in experiments.[16] Now, we consider time-varying A in Eqs. (12)–(13) to understand the mode transitions for the case with $\gamma_2 > \gamma_1$ and $k_2 > k_1$. P_2 is dominant for sufficiently small A. If A increases in time, it is expected that P_2 is more suppressed than P_1 because $k_2 > k_1$ means that P_2 is more sensitive to A than P_1, so P_1 can become dominant finally. Figs. 7–8 show the behaviors of $|P_2(t,0)|$ and $|P_1(t,0)|$ with growing A, supporting our prediction. Note that $|P_2(t,0)|$ is highly oscillating before convergence to 0 in Fig. 8, but not in Fig. 7. We should mention that the numerical examples presented here capture the importance of time-varying A and offer qualitative explanations for various types of mode transitions observed in experiments.

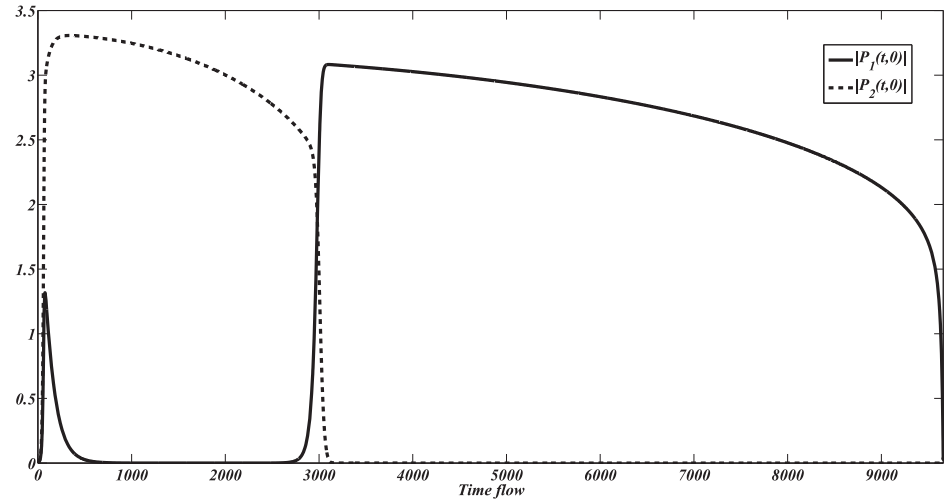

FIG. 7. The time behaviors of $|P_1(t,0)|$ and $|P_2(t,0)|$ for time-dependent $A(t)$ with $\eta = 1$, $k_1 = 1, k_2 = 3, \gamma_{L_1} = 10$, $\gamma_{L_2} = 11$, $\gamma_N = 1$ and $W(x) = \tanh(25x)$. We imposed weak initial conditions $P_1(0, x)$ and $P_2(0, x)$ as $(\gamma_{L_1}/\gamma_N)^{1/2}/1000$ and $(\gamma_{L_2}/\gamma_N)^{1/2}/1000$ respectively. A increases linearly, reaching the value 6.4393 at the end of the horizontal x-axis in the figure. First, $P_2(t, 0)$ is dominant and quasi-steady when the shear is small. As the shear increases beyond a critical value, $|P_1(t,0)|$ increases rapidly while $|P_2(t,0)|$ vanishes rapidly. After that, $P_1(t, 0)$ remains in a quasi-steady state until it falls to 0 abruptly.

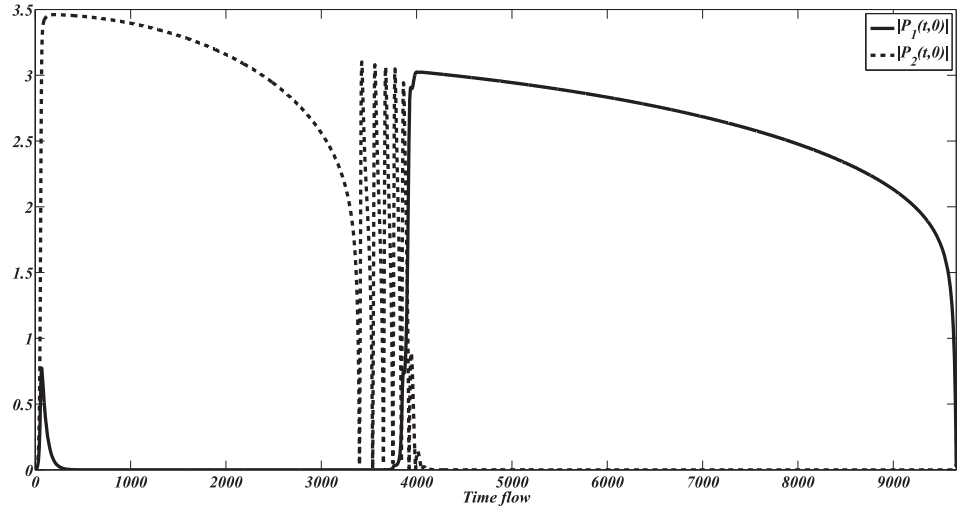

FIG. 8. The time behaviors of $|P_1(t,0)|$ and $|P_2(t,0)|$ for time-dependent $A(t)$ with $\eta = 1$, $k_1 = 1, k_2 = 3, \gamma_{L_1} = 10$, $\gamma_{L_2} = 12$, $\gamma_N = 1$ and $W(x) = \tanh(25x)$. We imposed weak initial conditions $P_1(0, x)$ and $P_2(0, x)$ as $(\gamma_{L_1}/\gamma_N)^{1/2}/1000$ and $(\gamma_{L_2}/\gamma_N)^{1/2}/1000$ respectively. A increases linearly, so A reaches to 6.4393 at the end of the horizontal x-axis in the figure. First, $|P_2(t,0)|$ is dominant when the shear is small. As the shear increases, $|P_1(t,0)|$ increases, but $|P_2(t,0)|$ decreases. After that, $|P_1(t,0)|$ act as a quasi-steady state, and finally, $|P_1(t,0)|$ falls to 0 abruptly. Compared to Fig. 7, it is also remarkable that the high oscillation of $|P_2(t,0)|$ before converging to 0 is observed.

IV. CONCLUSION

In summary, we considered two cases of ELM dynamics based on the extended complex GLE, Eq. (1). In the case of the single-mode, we studied the long-time behavior of the solution with fixed model coefficients and showed that the linear drive γ_L and the time-varying shear flow $A(t)$ determine the long time behavior of the solution. If the linear growth term is sufficiently large, the nonlinear oscillations are guaranteed for large shear flow. Conversely, the solution converges to a nonzero steady state for weak shear flow (Fig. 2). The long-time behavior for the small linear growth term is interesting because a solution converges to 0 for large flow shear (Fig. 1). Combining these results, we conclude that it is insufficient to consider the fixed coefficients on time to realize the quasi-steady states which are observed in experiments.[15] Therefore, by imposing time-varying shear flow, we obtained quasi-steady states numerically (Figs. 3–4). Note that the plasma rotation (flow) and its shear are well recognized as important factors for the stabilization of ELMs in MHD simulations, in particular for high toroidal mode numbers.[19–22] In recent nonlinear simulations using the nonlinear resistive MHD code JOREK for KASTAR H-mode plasmas,[22] it was shown that the shear of the self-consistent poloidal rotation profile becomes stronger toward the onset of ELM crash for the case of a single harmonic (eigenmode) simulation with the measured toroidal rotation profile.

Based on our numerical analysis, we expect that the quasi-steady mode can persist if the shear flow is reduced below the critical threshold by application of external magnetic perturbations, which may provide a candidate mechanism for the non-bursting quasi-steady modes in the ELM crash suppression experiment.[11]

To study the dynamics of coupled modes P_1 and P_2, we derived equations (12)–(13). We confirmed that the linear growth terms are crucial to determine the long-time behavior of P_1 and P_2 (Figs.5–6). Inspired by these results, we considered the increasing $A(t)$ on time and showed that rapid mode transition occurs (Figs.7–8), reproducing qualitatively the observed mode transitions in experiments.[16] Although we dealt with the equations (12)–(13) for coupled modes, it is also possible to obtain equations for more than two modes and show that each mode solution is successively dominant with suitable time-dependent $A(t)$.

Note that our extended complex GLE model does not resolve the trigger problem for the ELM crash because the model does not directly show the existence of non-modal solitary perturbation and

its burst (which initiates the pedestal collapse) observed in the experiments.[15,23,24] Nevertheless, the rapid disappearance of eigenmodes in our model may allude to a condition for the rapid unidirectional transition to the non-modal perturbation. In this regard, our model may be considered complementary to the existing trigger theory[25,26] and the nonlinear multi-harmonic simulations where the energy of the linearly dominant mode is redistributed into a broad spectrum as approaching to the ELM crash.[22,27,28]

To conclude, it is critical to consider the time-varying A for explanation of dynamic features in ELM phenomena using the given models (1) and (12)-(13) for single and coupled-modes, respectively.

ACKNOWLEDGMENTS

Hyung Ju Hwang was partly supported by the Basic Science Research Program through the National Research Foundation of Korea (NRF) (NRF-2017R1E1A1A030701051). M. Leconte was supported by R&D Program through National Fusion Research Institute (NFRI) funded by the Ministry of Science, ICT and Future Planning of the Republic of Korea (NFRI-EN1841-4). Gunsu S. Yun was partially supported by the National Research Foundation of Korea under grant No. NRF-2017M1A7A1A03064231 and by Asia-Pacific Center for Theoretical Physics.

APPENDIX: EXPLANATION OF WHY THE NONLINEAR OSCILLATION THRESHOLD IS INDEPENDENT OF *K*, FOR LARGE *K*

Notice that even if the shear $AW_K(x)$ appears, there exists a unique linearly stable steady state denoted by the superscript s, $P^s_{A,K} = R^s_{A,K} \exp\left(i\theta^s_{A,K}\right)$ such that $R^s_{A,K}(-x) = R^s_{A,K}(x)$ and $\partial_x\theta^s_{A,K}(x) = \partial_x\theta^s_{A,K}(-x)$ for small $A << 1$.[14] We can also deduce from (4)

$$\left.\frac{\partial\theta}{\partial x}\right|^s_{A,K} = \frac{A}{\eta}\int_{-1}^{x} W_K(x') \frac{R^s_{A,K}(x')}{R^s_{A,K}(x)} dx'. \tag{A1}$$

It should be checked how K affects the profile of $\left|P^s_{A,K}\right|$. It was numerically observed that there are stable symmetric stable steady states before $A < A_K$ (see Ref. 14). Due to

$$\lim_{K\to\infty} W_K(x) = \left\{ \begin{array}{c} -1 \text{ if } x<0 \\ 1 \text{ if } x>0 \end{array} \right\},$$

we can obtain

$$\begin{aligned} \left.\frac{\partial\theta}{\partial x}\right|^s_{A,K} &= -A\int_{-1}^{x} \frac{R^s_{A,K}(x')}{R^s_{A,K}(x)} dx' + A\int_{-1}^{x} \left(W_K(x')+1\right) \frac{R^s_{A,K}(x')}{R^s_{A,K}(x)} dx' \\ &\approx -A\int_{-1}^{x} \frac{R^s_{A,K}(x')}{R^s_{A,K}(x)} dx', \end{aligned} \tag{A2}$$

if $K >> 1$. Therefore, the equation (3) for $P^s_{A,K} = R^s_{A,K}\exp\left(i\theta^s_{A,K}\right)$ barely changes for $K >> 1$, so the profile of $\left|R^s_{A,K}(x)\right|$ is almost independent of K for $K >> 1$ due to (A2).

[1] L. Mestel, *Stellar magnetism*, Vol. 154 (OUP, Oxford, 2012).
[2] J. D. Murray, *Mathematical biology [electronic resource].: An introduction* (Springer, 2002).
[3] K. Burrell, "Effects of e × b velocity shear and magnetic shear on turbulence and transport in magnetic confinement devices," Physics of Plasmas **4**, 1499–1518 (1997).
[4] J. Cornelis, R. Sporken, G. Van Oost, and R. Weynants, "Predicting the radial electric field imposed by externally driven radial currents in tokamaks," Nuclear Fusion **34**, 171 (1994).
[5] R. Groebner, "An emerging understanding of H-mode discharges in tokamaks," Physics of Fluids B: Plasma Physics **5**, 2343–2354 (1993).
[6] R. Taylor, M. Brown, B. Fried, H. Grote, J. Liberati, G. Morales, P. Pribyl, D. Darrow, and M. Ono, "H-mode behavior induced by cross-field currents in a tokamak," Physical Review Letters **63**, 2365 (1989).
[7] F. Wagner, G. Becker, K. Behringer, D. Campbell, A. Eberhagen, W. Engelhardt, G. Fussmann, O. Gehre, J. Gernhardt, G. V. Gierke *et al.*, "Regime of improved confinement and high beta in neutral-beam-heated divertor discharges of the ASDEX tokamak," Physical Review Letters **49**, 1408 (1982).

[8] R. R. Weynants, G. Van Oost, G. Bertschinger, J. Boedo, P. Brys, T. Delvigne, K. Dippel, F. Durodie, H. Euringer, K. Finken *et al.*, "Confinement and profile changes induced by the presence of positive or negative radial electric fields in the edge of the textor tokamak," Nuclear Fusion **32**, 837 (1992).
[9] Y. Jeon, J.-K. Park, S. Yoon, W. Ko, S. Lee, K. Lee, G. Yun, Y. Nam, W. Kim, J.-G. Kwak *et al.*, "Suppression of edge localized modes in high-confinement KSTAR plasmas by nonaxisymmetric magnetic perturbations," Physical Review Letters **109**, 035004 (2012).
[10] A. U. Team, W. Suttrop, T. Eich, J. Fuchs, S. Günter, A. Janzer, A. Herrmann, A. Kallenbach, P. Lang, T. Lunt *et al.*, "First observation of edge localized modes mitigation with resonant and nonresonant magnetic perturbations in ASDEX upgrade," Physical Review Letters **106**, 225004 (2011).
[11] J. Lee, G. S. Yun, M. J. Choi, J.-M. Kwon, Y.-M. Jeon, W. Lee, N. C. Luhmann, Jr., and H. K. Park, "Nonlinear interaction of edge-localized modes and turbulent eddies in toroidal plasma under n= 1 magnetic perturbation," Physical Review Letters **117**, 075001 (2016).
[12] J. Connor, R. Hastie, H. Wilson, and R. Miller, "Magnetohydrodynamic stability of tokamak edge plasmas," Physics of Plasmas **5**, 2687–2700 (1998).
[13] M. Leconte, Y. Jeon, and G. Yun, "Ginzburg-Landau model in a finite shear-layer and onset of transport barrier nonlinear oscillations: A paradigm for type iii ELMs," Contributions to Plasma Physics **56**, 736–741 (2016).
[14] Y. Oh, G. S. Yun, and H. J. Hwang, "Mathematical analysis of long-time behavior of magnetized fluid instabilities with shear flow," arXiv:1706.08036 (2017).
[15] G. Yun, W. Lee, M. Choi, J. Lee, H. Park, B. Tobias, C. Domier, N. Luhmann, Jr., A. Donné, J. Lee *et al.*, "Two-dimensional visualization of growth and burst of the edge-localized filaments in KSTAR H-mode plasmas," Physical Review Letters **107**, 045004 (2011).
[16] J. Lee, G. S. Yun, M. Kim, J. S. Lee, W. Lee, H. Park, C. W. Domier, N. C. Luhmann, and W. H. Ko, "Toroidal mode number transition of the edge localized modes in the KSTAR plasmas," Nuclear Fusion **55**, 113035 (2015).
[17] L. Schmitz, L. Zeng, T. Rhodes, J. Hillesheim, E. Doyle, R. Groebner, W. Peebles, K. Burrell, and G. Wang, "Role of zonal flow predator-prey oscillations in triggering the transition to H-mode confinement," Physical Review Letters **108**, 155002 (2012).
[18] S. Jimbo and Y. Morita, "Stability of nonconstant steady-state solutions to a Ginzburg–Landau equation in higher space dimensions," Nonlinear Analysis: Theory, Methods & Applications **22**, 753–770 (1994).
[19] S. Saarelma, T. C. Hender, A. Kirk, H. Meyer, H. R. Wilson, and M. Team, "MHD stability analysis of ELMs in MAST," Plasma Physics and Controlled Fusion **49**, 31 (2007).
[20] L. E. Sugiyama and H. R. Strauss, "Magnetic x-points, edge localized modes, and stochasticity," Physics of Plasmas **17**, 062505 (2010).
[21] B. D. Dudson, X. Q. Xu, M. V. Umansky, H. R. Wilson, and P. B. Snyder, "Simulation of edge localized modes using bout++," Plasma Physics and Controlled Fusion **53**, 054005 (2011).
[22] M. Bécoulet, M. Kim, G. Yun, S. Pamela, J. Morales, X. Garbet, G. Huijsmans, C. Passeron, O. Février, M. Hoelzl, A. Lessig, and F. Orain, "Non-linear MHD modelling of edge localized modes dynamics in KSTAR," Nuclear Fusion **57**, 116059 (2017).
[23] R. Wenninger, H. Zohm, J. Boom, A. Burckhart, M. Dunne, R. Dux, T. Eich, R. Fischer, C. Fuchs, M. Garcia-Munoz *et al.*, "Solitary magnetic perturbations at the ELM onset," Nuclear Fusion **52**, 114025 (2012).
[24] J. Lee, G. Yun, W. Lee, M. Kim, M. Choi, J. Lee, M. Kim, H. Park, J. Bak, W. Ko *et al.*, "Solitary perturbations in the steep boundary of magnetized toroidal plasma," Scientific Reports **7**, 45075 (2017).
[25] S. C. Cowley, H. Wilson, O. Hurricane, and B. Fong, "Explosive instabilities: From solar flares to edge localized modes in tokamaks," Plasma Physics and Controlled Fusion **45**, A31 (2003).
[26] S. C. Cowley, B. Cowley, S. A. Henneberg, and H. R. Wilson, "Explosive instability and erupting flux tubes in a magnetized plasma," Proceedings of the Royal Society of London A: Mathematical, Physical and Engineering Sciences **471** (2015).
[27] I. Krebs, M. Hoelzl, K. Lackner, and S. Günter, "Nonlinear excitation of low-n harmonics in reduced magnetohydrodynamic simulations of edge-localized modes," Physics of Plasmas **20**, 082506 (2013).
[28] A. Mink, M. Hoelzl, E. Wolfrum, F. Orain, M. Dunne, A. Lessig, S. Pamela, P. Manz, M. Maraschek, G. Huijsmans, M. Becoulet, F. Laggner, M. Cavedon, K. Lackner, S. Günter, U. Stroth, and T. A. U. Team, "Nonlinear coupling induced toroidal structure of edge localized modes," Nuclear Fusion **58**, 026011 (2018).